Journal of Advances and Scholarly Researches in Allied Education
Vol. 12, Issue No. 2, January-2017, ISSN 2230-7540

An Study on Evaporation Residue Excitation Function For ^{16}o+^{194}pt Reaction

Sonu Rani[1]* Dr. Anil Kumar[2]

[1] Research Scholar of OPJS University, Churu, Rajasthan

[2] Associate Professor, OPJS University, Churu, Rajasthan

Abstract – In our present estimation, we gauged the ER excitation work for 16O + 194Pt at various research facility shaft energies. Standard measurable model figuring's utilizing Bohr-Wheeler splitting width under predicted the cross areas, particularly at higher excitation energies. In these counts, the dynamical impacts were excluded. With the presentation of dissemination into our counts, the cross segment expanded with increment in dispersal quality. Kramers' splitting width with dispersal coefficient n = 4 x 10-21 sec-1 repeated the ER cross segment at all energies agreeably. At lower energies, where splitting cross segment is a little division of aggregate combination cross area, the decrease in parting width did not roll out any apparent improvement in ER cross segment. In this area both the counts, accepting Bohr-Wheeler parting width and Kramers' width, yielded tantamount ER cross areas. Re-investigation of frameworks populating the composite frameworks 213,214Fr additionally yielded comparative outcomes.

Keywords: evaporation, residue, excitation function, 16o+194pt reaction.

----------X----------

INTRODUCTION

This paper is given to the examination and aftereffects of ER cross area estimations in 16O+194Pt response. Trial thinks about on splitting time sizes of hot cores have been done utilizing neutrons (G. K. Mehta 1988, D. Kanjilal 1993), charged particles (J. O. Stoner 2004, G. F. Meadow 1978) and GDR gamma beams (A. Breskin 1984, A. Jhingan 2010) as tickers. These analyses have demonstrated that the splitting rot is impeded over the desires dependent on the factual models. This backing off process was deciphered regarding a vast scale mass dissemination process including the impacts of atomic thickness (T. K. Ghosh). This brought about a dynamical portrayal of splitting procedure consolidating atomic dissemination into record. Significant disadvantage with these timekeepers is that they are not extremely touchy to whether the emanations happen previously or after the traversal of the seat point, as the framework continues towards scission. On the other hand vanishing likelihood of a hot core delivered in an overwhelming particle crash is delicate just to the dispersal quality inside the splitting hindrance. In the event that the splitting branch is stifled because of dissemination, there is an unequivocally improved survival likelihood for the ERs. This will be showed as an expansion in ER traverse the expectations of factual models. It is additionally announced that the exploratory combination cross areas in mass ~ 200 district is altogether lessened notwithstanding for exceptionally deviated responses, because of the beginning of various non-compound core forms. Dissipation deposits (ER) are the unambiguous marks of CN arrangement and can be utilized as a touchy test to ponder the factual and also dynamical parts of combination splitting responses. In this part we talk about the information investigation technique, another strategy to acquire the transmission proficiency of HYRA, measurable model estimations and results. Re-investigation of a few frameworks revealed in writing in same mass area is talked about toward the finish of the part.

DATA ANALYSIS

1. ER Cross Area

The aggregate ER cross area can be figured utilizing the basic articulation

$$\sigma_{ER} = \frac{Y_{ER}}{Y_{mon}} \left(\frac{d\sigma}{d\Omega}\right)_R \Omega_M \frac{1}{\eta_{HYRA}} \qquad (5.1)$$

whereaER is the ER cross area in mb, YER is the ER yield at the central plane, Ymon is the yield in the screen finder, nHYRA is the HYRA transmission effectiveness of HYRA and is the soild point subtended by the screen detector. Is the differential

Rutherford diffusing cross area in the research facility framework,

$$\left(\frac{d\sigma}{d\Omega}\right)_R = 1.296\left(\frac{Z_P Z_T}{E_{lab}}\right)^2\left[\frac{1}{sin^4\left(\frac{\theta}{2}\right)} - 2\left(\frac{M_P}{M_T}\right)^2 + \ldots\right] \quad (5.2)$$

where ZP and Zp are the nuclear number of the shot and target, separately and 9 is the screen finder edge as for shaft course. MP and Mp are the mass of the shot and target, individually.

2. Transmission productivity

Transmission productivity is the proportion of the quantity of ERs achieving the central plane to their aggregate number delivered at the objective chamber, amid the communication procedure. nHYRA relies upon different parameters, for example, vitality of the ER, entrance channel mass asymmetry, target thickness, precise conveyance of the ERs and henceforth the rakish acknowledgment of the separator, gas weight, attractive field settings, size of the central plane indicator and so on. Passageway channel mass asymmetry, rakish acknowledgment of the separator, target thickness and size of the central plane locator stay unaltered amid a test. The attractive field esteems were advanced for most extreme transmission in every vitality. From our prior adjustment runs we seen that the reliance of gas weight won't change the transmission apparently in the vitality scope of intrigue. The gas weight was set at the upgraded esteem and was not changed with vitality, amid the examination. Gas filled separators offer better transmission proficiency over vacuum spectrometers because of the charge state and speed centering. Be that as it may, transmission proficiency estimations utilizing regular gamma beam strategy was most certainly not for all intents and purposes extremely encouraging in this estimation, because of the exceptional gamma foundation beginning from the splitting parts and in addition from the response results of the bar with the weight window thwart (nickel). In the gamma strategy, gamma beams from the responses were recorded in incident with ER and furthermore in singles. The proportion of a particular gamma line in occurrence range to that in singles range gives the outright transmission effectiveness. Be that as it may, in the present estimation, the singles range was debased by gammas from different causes as specified previously. This made the strategy for all intents and purposes difficult to quantify the transmission productivity. Thus, an alternate strategy was pursued to get the nHYRA, for 16O+194Pt response.

In this strategy, we utilized 16O+184W as the alignment response. The ER cross area for 16O+184W framework was estimated prior utilizing the vacuum mode spectrometer HIRA (N. Madhavan 2010). The ER cross area for this framework had been estimated at 96.0 MeV bar vitality. For this estimation, isotopically advanced 184W (210 ^g/cm2 thick on 110 ^g/cm2 thick carbon backing, with carbon confronting the shaft) target was mounted on the objective step. The initial phase in this strategy was to ascertain nHYRA for 16O+184W framework. This was in certainty stright forward as the exploratory ER cross segment was known for this framework and other experimental parameters in Eq. 4.1 were likewise known. The transmission effectiveness of a gas filled mass separator relies on the extent of the central plane indicator. As examined previously, we utilized a MWPC pursued by a two-dimensional silicon identifier at the central plane with dynamic territory 47 x 47 mm2 and 40 x 40 mm2, separately. Consequently the n esteems were distinctive for these two identifiers, relative to their dynamic region. We here make a gauge of n esteems with both the locators. Nonetheless, in the last cross area estimations, we utilized the ER checks from the silicon identifier and thus the n esteem for this finder. Eq. 4.1 can be re-composed as,

$$\eta_{HYRA} = \frac{Y_{ER}}{Y_{mon}}\left(\frac{d\sigma}{d\Omega}\right)_R \Omega_M \frac{1}{\sigma_{ER}} \quad (5.3)$$

Substituting the ER counts (from MWPC identifier) and other quantities, the n value for 16O+184W reaction (nmwRA) was observed to be 2.48 ± 0.40 %. The estimation of n got with the ER tallies taken from the silicon locator (nHvRA) was 1.78 ± 0.27 %. Here aER is the ER cross segment as got in the before work (N. Madhavan 2004).

The next step was to extract n HYRA esteem for 16O+194Pt reaction from the esteem acquired for 16O+184W reaction. Since the previous response is more unbalanced, the precise conveyances of the ERs delivered in this response will be not the same as that of the last response.

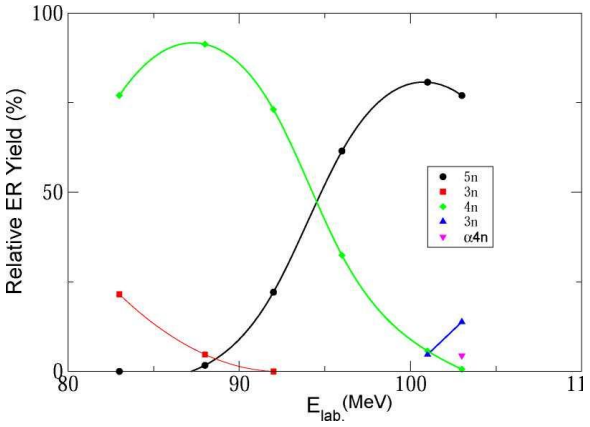

Figure 4.1: PACE3 results for the population of different exit channels in the complete fusion of ^{16}O with^{194}Pt at different laboratory beam energies. Relative yield of each ER was shown as a percentage of total ER cross sections. Only channels

with relative yield greater than 1% were considered while plotting.

Table 4.1: PACE3 results for population of major exit channels in the complete fusion of ^{16}O with ^{194}Pt at different laboratory beam energies. Relative yield of each ER was shown as a percentage of total ER cross sections.

E_{ia6}(MeV)	3n (%)	4n (%)	4n (%)	6n (%)	*aAn* (%)
83.7	21.4	77.0			
87.8	4.72	91.3	1.7		
91.9		73.1	22.1		
96.0		32.4	61.4		
101.1		4.7	80.7	4.7	
103.1			77	13.8	4.4

Table 4.2: n values of HYRA for $^{16}O+^{194}Pt$ system at different beam energies.

$E_{lab}(MeV)$	$VH^{b}{}_{Y}{}^{d}RA$ (%)	*Vh7ra*(%)
101.1	1.64 ± 0.24	2.29 ±0.34
96.0	1.60 ±0.24	2.24 ±0.34
91.9	1.48 ±0.24	2.21 ±0.33
87.8	1.46 ±0.23	2.18 ±0.33

The more uneven the response is, bigger will be the rakish spread of the ERs. Clearly n (of any spectrometer) relies upon the precise acknowledgment of the spectrometer. The precise dissemination of the ERs created in 16O+184W and 16O+194Pt were reproduced utilizing the semi-minuscule Monte Carlo code TERS [14, 14]. TERS produces the reasonable estimations of ER parameters, for example, removal, rakish dissemination, charge state appropriation, vitality circulation and so on, occasion by occasion. Factual model code PACE3 was utilized to check the significant rot directs in 16O+184W response at 96.0 MeV. As per PACE3 forecast xn-channels were the predominant rot directs in this response (4n channel (9.7%), 4n channel (79%) and 6n channel (6.7%). The amount inside the section is the relative ER yield as for aggregate ER cross segments). Consequently the precise dispersions were mimicked for all the three neutron vanishing channels and standardized (weighted normal) to get the rakish conveyance of aggregate ERs created in this response. The predominant rot diverts in 16O+194Pt response were additionally computed utilizing PACE3 for various shaft energies contemplated in the test. Fig. 4.1 demonstrates the PACE3 results for thepopulation of various leave diverts in the entire combination of 16O+194Pt response at various lab bar energies. Relative yield of every ER is appeared as a level of aggregate ER cross areas. Just channels with relative yield more prominent than 1% were considered while plotting. It might be seen that the rot channels are ruled by neutron vanishing and the commitment from proton dissipation and a molecule dissipation are insignificantly little. At the most elevated vitality (103 MeV), a molecule dissipation begins to add to the rot. On the off chance that a-vanishings were available even at lower energies, it would have been extremely hard to separate nHYRA for 16O+194Pt response as the a-dissipation results bigger spread in the precise dissemination of ERs. Table 4.1 gives the relative yield (in rate) of real leave diverts in the total combination of 16 O with 194Pt at various research facility shaft energies anticipated by PACE3. The precise disseminations of the prevailing rot channels at 96.0 MeV vitality were recreated for 16 O+194Pt response and aggregate rakish appropriation of ERs were acquired likewise utilized before for 16 O+184W response. A similar method was pursued for the rot channels at different energies too.

The ERs delivered in substantial particle crashes for the most part peack around 0o (forward focused). Be that as it may, if the objective is thick, various dissipating impacts prompt bigger precise spread of ERs. The dissipation of particles from the CN and ERs further spread the rakish circulations. Despite the fact that the objective thickness can be decreased to stay away from various scrambling occasions extensively, the spread because of molecule vanishing can't be controlled using any and all means by the experimenter. Rakish dispersion relies upon the passageway channel mass asymmetry too. Heavier the shot, more forward focused will be the ERs delivered. Consequently, to separate n HYRA for 16O+194Pt response from 16O+184W response, the rakish acknowledgment of the spectrometer for both the response items must be considered. The gap of the main quadrupole (with an internal span of 96 mm) was constraining the precise acknowledgment of HYRA in our present measurements, with an acknowledgment point ± 9.6o. The standardized rakish conveyances of ERs from 16O+194Pt and 16O+184W responses at various pillar energies are appeared in Fig. 4.2. From Fig. 4.2, examination of the rakish dispersions were made for the two responses, inside the acknowledgment of HYRA at 96.0 MeV pillar vitality. The region of the standardized precise appropriation bend of 16O+194Pt response at 96 MeV was approximately 10% not as much as that of 16O+184W at a similar vitality. The decrease in zone was normal for this framework, attributable to its more unbalanced passageway channel contrasted with 16O+184W response. Thus a factor 0.9 was utilized to increase the transmission productivity of HYRA, nHYRA, for 16O+184W reaction to get nnYRA for 16O+194Pt response at this vitality. Comparative examinations were made for different energies to get their relating increase factor. Preferably one needs to gauge nHYRA for all energies, which isn't practicable. Table 4.2 shows nHYRA esteems figured for the silicon identifier and in addition for MWPC at

various bar energies in 16O+194Pt response. It might be noticed that the variety in n esteems are not exceptionally huge with vitality and are well inside the blunder bars. Subsequently, in our figurings we utilized nHYRA = 1.60 ±0.24% in all energies to acquire without a doubt the cross segments.

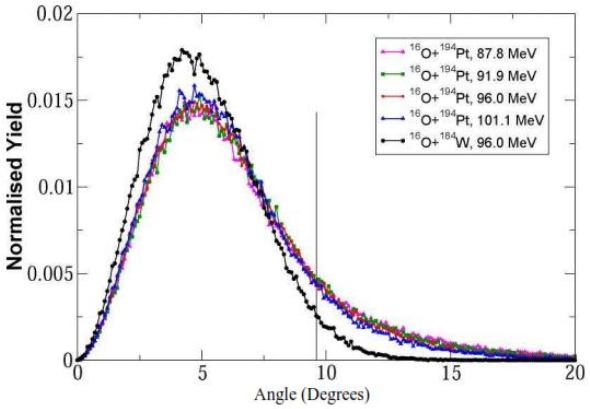

Figure 4.2: The normalized angular distributions of ERs in ^{16}O+^{194}Pt and ^{16}O+^{184}W reactions simulated using the Monte Carlo code TERS. The line at 9.6^{o} indicates the angular acceptance of HYRA.

RESULTS

Experimental ER cross sections were calculated using Eq. 4.1. ER counts from the two-dimensional

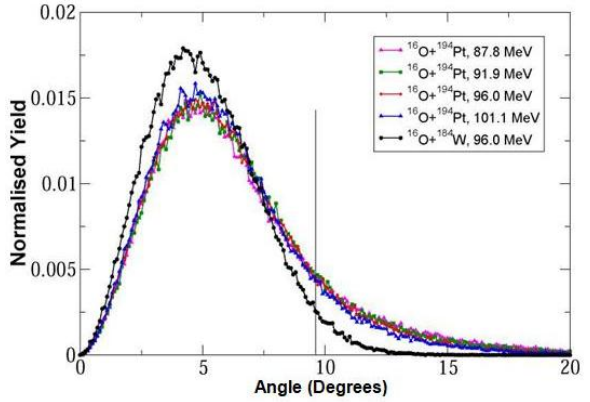

Table 4.3: Measured ER cross section function of $E_{c\cdot m}$..

$E_{c\cdot m}$.(MeV)	$o_E r$ (mb)	*oer* error (mb)
69.7	4.4	0.9
73.4	44.0	9
77.3	168.1	29.0
81.1	214.0	38.1
84.9	218.0	33.0
88.7	241.0	39.0
93.4	218.0	33.2
94.2	174.0	31.0

Two dimensional silicon locator was utilized for cross segment estimations with nnYRA = 1.60 ±0.24%. Table 4.3 demonstrates the deliberate ER cross area as a component of focus of-mass vitality, Ec.m.. Out of the considerable number of amounts in Eq. 4.1, nHYRA contributes the greatest in by and large mistake in the last cross area. The factual blunder in every identifier yield is given by where N is the quantity of tallies. While taking the aggregates and proportions of the locator checks, the standard mistake proliferation equation.

$$\sigma_u = \sqrt{\left(\frac{\partial u}{\partial x}\right)^2 \sigma_x^2 + \left(\frac{\partial u}{\partial y}\right)^2 \sigma_y^2} \qquad (5.4)$$

was utilized for ascertaining the blunder associated with the determined amounts. The mistakes in the estimations of the locator strong points and precise position of the finders were likewise incorporated into the computations alongside factual blunders.

It might be noted from Table 4.3 that ER cross area increments with shaft vitality, immerses at higher energies. At the most noteworthy vitality, cross area even shows a declining pattern. This might be because of the way that splitting cross area winds up predominant at higher excitation energies.

4. Statistical model examination

Measurable ideas and models have been utilized in atomic science since its start. The core is a many-body, complex framework which, whenever given even a fairly little measure of excitation vitality, may encounter a wide range of designs. The thickness of quantum-mechanical states increments quickly with excitation vitality and before long turns out to be extensive. Indeed, even at the most minimal shelling energies at which atomic responses can be started with charged particles, there are numerous states accessible for the CN and a wide range of ways it can rot. In such a perplexing circumstance, factual techniques are fundamental for the appreciation and expectation of numerous atomic marvels. In combination responses the CN will be shaped with high excitation vitality and precise momenta. Such a hot, quickly pivoting framework experience fast rot to its ground state through different rot channels. Molecule discharge and parting contend first and foremost. The molecule discharge and parting can occur from the CN itself or from the rot items. At the point when the excitation vitality turns out to be not exactly the molecule division vitality and splitting boundary, gamma rot assumes control over the rot procedure. The rest of the excitation vitality and precise force will be expelled thusly. Measurable models accept that all possibiliteis for rot are, characteristically, similarly likely. Henceforth, these conceivable outcomes are administered by elements, for example, the thickness of the last states and boundary infiltration factors. The likelihood for a specific rot to happen is contrarily relative to the

aggregate number of conceivable rots. This factual presumption, when joined with protection laws and guideline of point by point balance, prompts a measurable model for normal cross areas. Today measurable models find wide application. These models can be utilized to confirm the response system, to help in the rot of CN development and rot, to decide rakish momenta, and to seek non-measurable parts of atomic structure at high excitation energies and precise momenta.

4.1 The model

The CN shaped in combination splitting response rot through two noteworthy channels, molecule emis¬sion and parting. In splitting procedure, the overwhelming CN parts into two sections. Amid the entry of the middle composite framework from balance misshapening to saddle point and from seat point to scission point, the emanation of particles and gamma quanta proceeds. The particles discharged before scission point are called pre-scission particles. Indeed, even after splitting the sections are still in energized states and dissipate particles, which are called post-scission particles. In measurable model, the discharge of these light particles and GDR gamma beams have been considered as rot channels for the energized CN notwithstanding the splitting channel. The procedure of light molecule discharge from a CN is represented by the outflow rate T" at which a particle of sort v is radiated at a normal vitality in the range before parting. The incomplete rot widths rv for emanation of a light molecule of sort v is given by Wiesskopf equation sv is the turn of the radiated molecule v, mv is the lessened mass concerning the remaining core, Bv is the coupling vitality of the produced molecule ascertained utilizing the LDM, Eint is the inborn excitation vitality of the parent core, ev is the vitality of the transmitted molecule and AERot is the change in rotational vitality because of the precise energy diverted by the discharged molecule. pc(Eint) and pR are the dimension densities of the CN and lingering cores, separately. ainv(ev) is the converse cross segment. The dimension thickness of the remaining cores is given by,

$$\Gamma_\nu = (2s_\nu+1)\frac{m_\nu}{\pi^2\hbar^2\rho_c(E_{int})}\int^{E_{int}-B_\nu-\Delta E_{Rot}} d\epsilon_\nu \rho_R(E_{int}-B_\nu-\Delta E_{Rot}-\epsilon_\nu)\times\epsilon_\nu\sigma_{inv}(\epsilon_\nu) \quad (5.5)$$

where is the snapshot of latency and J is the rakish force of the turning framework. The dimension thickness parameter has been taken from crafted and is given as pursues:

$$\rho_R(E_{int},A,J) = (2J+1)\Big[\frac{\hbar^2}{2\Im_0}\Big]^{\frac{3}{2}}\frac{\sqrt{a}}{12}\frac{exp(2\sqrt{aE_{int}})}{E_{int}^2} \quad (5.6)$$

where U is the thermal energy of the CN, An is the shell correction at ground state deformation, obtained by taking the difference of experimental and liquid drop masses, n is the damping factor, which is a measure of rate at which shell effects melts away with increase in excitation energy and *a* is the asymptotic value to which the level density parameter approaches with increase in excitation energy. The inverse cross sections are given by

$$a(U) = \overline{a}\big[1+\frac{\Delta n}{U}(1-e^{-\eta U})\big] \quad (5.7)$$

$$\sigma_{inv}(\epsilon_\nu) = \begin{cases} \pi R_\nu^2(1-V_\nu/\epsilon_\nu) & \text{for } \epsilon > V_\nu \\ 0 & \text{for } \epsilon < V_\nu \end{cases}$$

with

$$R_\nu = 1.21\Big[(A-A_\nu)^{\frac{1}{3}}+A_\nu^{\frac{1}{3}}\Big]+(\frac{3.4}{\epsilon_\nu^{1/2}})\delta_\nu \quad (5.8)$$

Where A_v is the mass of the emitted particle. V_v is the Coulomb barrier calculated using the expression,

$$V_\nu = \frac{\Big[(Z-Z_\nu)Z_\nu K_\nu\Big]}{R_\nu+1.6} \quad (5.9)$$

It may be remembered that Coulomb barrier is zero for neutrons. K_v = 1.32 for *a* particles and deutrons and 1.14 for protons. Lynn formula was used for GDR gamma widths, given by

$$\Gamma_\gamma = \frac{3}{\rho_c(E^*)}\int_0^{E_{int}-\Delta E_{Rot}} d\epsilon\rho_R(E_{int}-\Delta E_{Rot}-\epsilon)f(\epsilon) \quad (5.10)$$

with

$$f(\epsilon) = \frac{4}{3\pi}\frac{(1+\kappa)}{mc^2}\frac{e^2}{\hbar c}\frac{NZ}{A}\frac{\Gamma_G\epsilon^4}{(\Gamma_G\epsilon)^2+(\epsilon^2-E_G^2)^2} \quad (5.11)$$

Where *k* = 0.74, E_G and r_G are the position and width of the GDR, respectively. Finally, the fission width has been taken from thetransition-state model.

$$\Gamma_{BW} = \frac{1}{2\pi\rho_g(E_i)}\int_0^{E_i-V_B}\rho_s(E_i-V_B-\epsilon)d\epsilon \quad (5.12)$$

wherep_g is the level density at the initial state (Ej, Jj) and p_s is the level density at the saddle point. Vs is the fission barrier. Under the condition ^<cl and assuming the [E]ilevel density parameter at the ground state and saddle point to be the same and further assuming a simplified form of *p(E)* ~ exp(2\/aE)$_1$ the Bohr-Wheeler width reduces to

$$\Gamma_{BW} = \frac{T}{2\pi} e^{(-V_B/T)} \qquad (5.13)$$

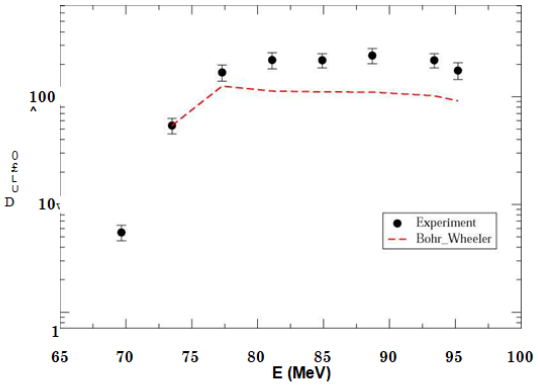

Figure 5.3: The experimental ER cross section compared with statistical model calculations assuming Bohr-Wheeler fission widths.

By utilizing the widths of all the rot modes clarified in detail over, the time advancement of a CN was followed in the factual model code until either splitting happens or an ER is framed. The calculations have been performed over an expansive number of gatherings. The combination turn circulation (CN turn conveyance) was utilized as the contribution to the model in the computations. This CN turn appropriations were acquired utilizing the coupled channel code CCFULL [21] subsequent to repeating the test add up to combination cross segments (aggregate of ER cross segment and splitting cross area). The splitting cross areas in 16O + 194Pt at various pillar energies were estimated in a different test, examined in section 6. Rotational couplings of the objective cores were likewise incorporated into the counts. The obstruction parameters of the code CCFULL were settled by coordinating the combination excitation capacities. As we had splitting cross segment information just upto 90 MeV, at higher energies, we were compelled to consider the turn disseminations anticipated by CCFULL in our estimations. In any case, it might be made reference to that there was no peril in this supposition, as the CCFULL parameters were at that point settled at energies underneath 90 MeV. At energies well over the Coulomb boundary, the channel coupling impacts are similarly immaterial. In Fig. 4.3, we have contrasted the trial ER excitation work and the measurable model calcula¬tions accepting Bohr-Wheeler parting widths. The model estimations did not consider any dynamical highlights and accordingly underprediced the ER cross segments at higher energies.

4.2 Calculations consolidating dynamical impacts

Atomic splitting is an exemplary case of moderate vast scale aggregate movement. The standard measurable model of Bohr and Wheeler was adequate for quite a while to portray the watched impacts of atomic parting till the availabilty substantial particle pillars. Trial information from different overwhelming particle actuated responses have brought about the perception of un¬expectedly substantial pre-scission yields of charged particles, neutrons and GDR gamma beams over the expectations from the standard factual model. This underestimation of pre-scission particles at higher excitation energies by the measurable model driven examiners to believe that adequate time was not accessible for the particles to vanish before splitting. At lower excitation energies, the measurable model calcu¬lations hold great on the grounds that in this vitality run, the molecule variety has insignificant reliance on parting width. Be that as it may, with increment in excitation vitality, splitting width increments and winds up practically identical to the molecule emanation widths and the reliance of molecule assortment on parting width ends up noteworthy. The perception of this backing off of splitting procedure in respect to the desires for the standard factual model was translated regarding an extensive scale mass dissemination process including the impacts of atomic thickness. P. D. Shidling (2006) brought up that splitting rot width, normally given by the Bohr-Wheeler articulation decided at the seat point, is diminished by the dissemination procedure in light of the fact that the last makes the transition be reflected back at the sad¬dle point. This upgrades the discharge of particles and gamma beams before the framework goes through its seat point. Atomic scattering further backs off the movement of the composite framework on its way from seat point to scission arrangement, in this manner expanding the rot likelihood of particles and gamma beams between the seat to scission change. The decrease in splitting width can prompt an expansion in the sur¬vivalprobabilty of the ER. This will be showed in an improved ER cross area.

The Kramers' splitting width is given by,

$$\Gamma_{Kramers} = \Gamma_{BW} \times (\sqrt{1+\beta^2} - \beta) \qquad (5.14)$$

whereft is the atomic grinding coefficient, ft = n/2ws. n signifies the decreased scattering coefficient and us means the potential bend at the seat point. Eq. 4.14 can be composed as

$$\Gamma_{Kramers} = \frac{\hbar\omega_g}{2\pi} e^{(-V_B/T)} \left\{ \sqrt{1 + \left(\frac{\eta}{2\omega_s}\right)^2} - \frac{\eta}{2\omega_s} \right\} \qquad (5.15)$$

We discovered that the measurable model computations utilizing Bohr-Wheeler parting width underpredict the ER cross segments at higher excitation energies. This might be because of the beginning of dynamical impacts, which postpone the parting rot. Consequently, with the end goal to clarify the upgraded ER cross area, atomic dissemination must be mulled over in the counts. We played out the model figurings with Bohr-Wheeler splitting width supplanted by Kramers' width with various n

esteems. The counts utilizing n = 4 x 10-21 sec-1 replicated the ER cross areas palatably, particularly at higher excitation energies. In Fig. 4.4, we contrasted the test ER excitation work and the measurable model estimations expecting Kramers' splitting widths. Counts utilizing Bohr-Wheeler splitting width and aggregate combination cross area computed utilizing coupled channels code CCFULL are likewise appeared. Table 4.4 shows different amounts computed utilizing factual models in the present investigation.

Table 4.4: Various quantities calculated using statistical model for ^{16}O + ^{194}Pt as a function of $E_{c\cdot m}$..<x§W and ff|™^{mers} are the ER cross sections calculated using BohrWheeler fission width and Kramers' fission width, respectively. Similarly off's and $^{a}fisS^{mers}$ are the fission cross sections calculated using Bohr-Wheeler fission width and Kramers' fission width, respectively.

E_c.m. (MeV)	(mb)	(mb)	—*Kramers*$^{a}ERl^{mD}$J	—*Kramers* fry-jEW$^{a}fiss$ \$^{Ili[}J	U *fusion*
73.4	44.0	24.4	64.3	14.1	78.4
77.3	124.3	138.3	142.1	121.4	263.6
81.1	112.8	333.9	163.7	283.0	446.8
84.9	110.8	499.4	200.7	409.6	610.3
88.7	110.2	647.8	227.9	430.2	748.0
93.4	101.9	816.7	237.3	681.3	918.6
94.2	91.4	883.3	226.2	748.4	974.7

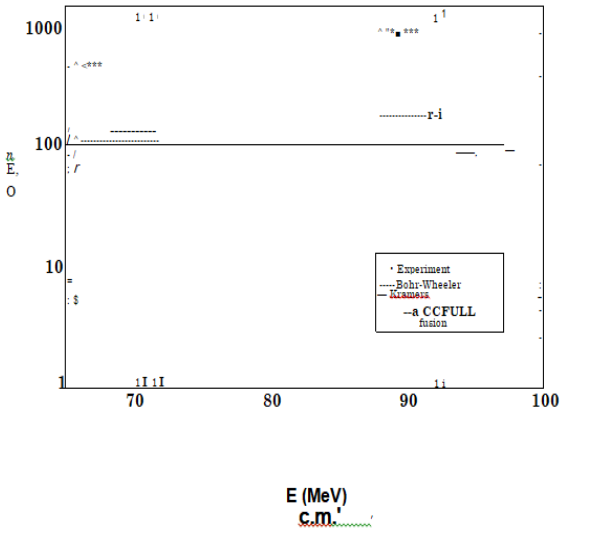

Figure 5.4: The experimental ER cross section compared with statistical model calculations assuming Bohr-Wheeler and Kramers' fission widths. Total fusion cross section calculated by coupled channels code CCFULL is also shown.

Calculations for some adjacent frameworks detailed in writing

Our present ER excitation estimations demonstrated the impact of atomic dissemination in combination elements in mass ~ 200 area. It was discovered that n = 4 x 10-21 sec-1 satisfactorily duplicates the ER cross area at all energies. Comparable outcomes were accounted for before by A. Jhingan (2004) in 16O+184W and 19F+181 Ta, framing the CN 200Pb. It was accounted for that dissipative power with quality fl = 3 replicated the ER cross area for 16O+184W response and fl in the range 1 to 3 was required for fitting the excitation work for 19F+181Ta response. It will intrigue further stretch out this investigation to frameworks for which ER cross segments are accounted for, especially in ~ 200 mass area.

4.1 16O+197Au response

The ER cross segments in 16O+197Au framework were estimated by N. Madhavan (2004). The creators watched an improvement in ER cross area at higher excitation energies. Measurable model figurings were performed utilizing the adjusted rendition of CASCADE. In their examination, the measurable model parameters were differed with the end goal to discover the parameter set that recreates the cross segment. The vital three parameters are the tallness of the parting hindrance, communicated through a scaling factor kf to Sierk obstruction; the proportion of level thickness parameters between seat point and harmony shapes, af/a; the dimension thickness parameter at balance disfigurement, an. Every one of these three parameters were shifted autonomously, keeping the other two at their ostensible qualities (i.e., kf — 1, af/a — 1 and a — A/(9 MeV), individually). The factual parameter sets detailed by Brinkman et al [23], yielding agreeable repro¬duction of the deliberate ER excitation works beneath 100 MeV are appeared in Table 4.4

As various arrangements of factual parameters anticipated the ER cross segment in this response sensibly well at energies beneath 100 MeV, we chose to re-break down the information utilizing our model. The combination turn dispersions were ascertained utilizing CCFULL. Combination cross segments (entirety of ER and parting cross areas) were fitted utilizing CCFULL for getting the combination turn conveyances. The parting cross segments were taken from B. P. AjithKumar (1997). The low lying aggregate conditions of the objective cores were incorporated into the coupled channel figurings for duplicating the cross areas at close obstruction energies. We discovered that factual model counts expecting Bohr-Wheeler parting width belittle the ER cross segment at all energies with the exception of the most minimal vitality. Computations utilizing Kramers' parting width, with a dissemination coefficient n — 4 x 10-21 sec-1 recreated the ER cross segment attractively at higher energies. Consequently we could succesfully clarify the improvement of ER traverse the expectations from the factual model counts accepting Kramers' splitting width by fusing the atomic dissipative impacts. In Fig. 4.4, we contrasted the test ER excitation work and the measurable model estimations expecting Kramers' splitting widths. Figurings utilizing Bohr-Wheeler parting width and aggregate combination cross area

ascertained utilizing CCFULL are likewise appeared in the figure.

Table 5.5: The statistical parameter sets reported by Brinkman et al [23], yielding satisfying reproduction of the measured ER excitation functions below 100 MeV.

k/		A/a$_n$
1.05	1	9
1.0	0.98	9
1	1	10.0

4.2 18O+197Au response

Measurable computations were additionally performed for 18O+197Au response shaping the CN 214Fr. ER cross segments for neutron dissipation channels were just accessible from this reference and aggregate cross segment was taken as the whole of these neuton channels. Different channels were observed to be unimportantly little in adding to the aggregate ER cross area. We, thus disregarded these channels as the blunder bars announced in the ER estimation itself was ±20. The parting cross segments were taken from A. K. Sinha (2010). CCFULL was utilized to repeat the test combination cross segments and combination turn appropriations. The low lying aggregate conditions of the objective cores were incorporated into CCFULL computations. It might be noticed that parting cross areas were accessible upto focus of-mass vitality

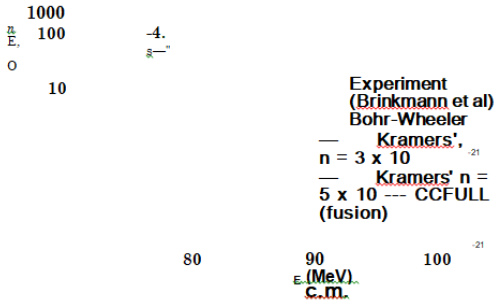

Figure 5.5: The experimental ER cross section in $^{18}O+^{197}Au$ system compared with statistical model calculations assuming Bohr-Wheeler and Kramers' fission widths. Total fusion cross section calculated using CCFULL are also shown.

88.4 MeV as it were. Thus at energies above 88.4 MeV, add up to combination cross segments and combination/ - circulations were taken from CCFULL forecasts as it were. As specified before, at energies well over the Coulomb hindrance, the channel coupling impacts are not noteworthy. Table 4.6 records the CCFULL parameters utilized for the estimation of combination turn disseminations for the three responses 16O + 194Pt, 16O + 197Au and 18O + 197Au. As in the past two cases, demonstrate figurings utilizing Bohr-Wheeler splitting width underpredicted the aggregate ER cross segment in 18O + 197Au response. In Fig. 4.6, trial ER excitation work is contrasted and the measurable model figurings. Add up to combination cross segment ascertained utilizing CCFULL is additionally appeared in the figure.

Table 4.6: CCFULL parameters used in $^{16}O + ^{194}Pt$, $^{16}O + ^{197}Au$ and $^{18}O + ^{197}Au$ reactions.

Reaction	V_0 (MeV)	a_0 (fm)	r_0 (fm)
$^{16}0 + ^{194}Pt$	64.4	0.6464	1.2
$^{16}0 + ^{197}Au$	64.4	0.647	1.2
$^{18}0 + ^{197}Au$	64.2	0.661	1.2

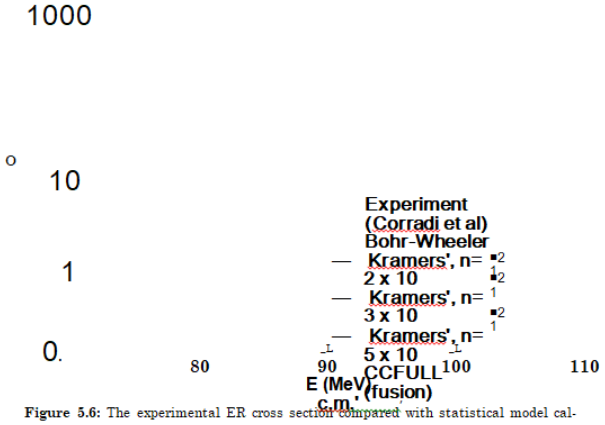

Figure 5.6: The experimental ER cross section compared with statistical model calculations for $^{18}O + ^{197}$ reaction. Total fusion cross section calculated using CCFULL is also shown.

CONCLUSION

The investigation of exceptionally energized combination splitting response in mass ~ 200 area has developed as a subject of extraordinary enthusiasm for ongoing years. In this mass locale splitting rot dependably contends with molecule vanishing. Trial estimations utilizing different tests, for example, neutron, charged molecule and gamma beam multiplicities demonstrated that the parting procedure is deferred over the expectations from the standard factual models. This backing off, frequently called as splitting prevention was credited to the dynamical effetcs in the combination procedure. It, thusly, gives the idea that a dynamical model including dissemination would give a superior portrayal of the splitting wonder at high excitation energies. On the off chance that we experience writing, not very many estimations on ERs have been completed to address this marvels. It might be made reference to that when the melded composite framework moves from harmony distortion to scission arrangement through seat point, it continuosly emanates the particles and gamma beams. Thus these molecule and gamma multiplicities are not extremely delicate to whether the outflows happen previously or after the traversal of the seat point. In any case, the ER likelihood from a hot core is touchy to the dissemination quality inside the splitting hindrance. Dissemination improves the survival probabilty of the CN against splitting. This would result in an improved ER cross area. The destiny of the CN, i.e., regardless of whether it will experience parting or make due as an ER is predominantly chosen inside the seat point. Subsequently, ER estimations can give profitable data about pre-saddle scattering.

It was additionally detailed that the trial combination cross segments in mass ~ 200 area is altogether decreased notwithstanding for exceptionally hilter kilter responses, because of the beginning of different non-compound core forms. These non-compound core forms incorporate quick splitting, pre-balance parting and quasifission. Quick parting happens when the precise energy populated is high to the point that the splitting boundary vanishes. At the point when there is no parting obstruction, the composite framework won't be caught and experiences unavoidable re-division. Pre-balance parting happens for the frameworks in which the splitting hindrance winds up tantamount to the atomic temperature. Quasifission, the third non-harmony process was anticipated for heavier shot target mixes by the dynamical models proposed couple of decades back. These models anticipated the beginning of quasifission just when the charge item ZPZT > 1600. Be that as it may, ongoing estimations uncovered a solid passageway channel reliance for this procedure, particularly on mass asymmetry and misshapening of the response accomplices. Beginning of quasifission was accounted for notwithstanding for extremely topsy-turvy frameworks with low ZPZT esteems. Marks of quasifission watched for 24Mg + 186W response in our estimation was talked about in part 4. Be that as it may, splitting piece mass conveyance estimations for 16O + 194Pt demonstrated that the framework continued through evident CN arrangement. The beginning of non-harmony forms decrease the survival probabilty of ERs against re-detachment and diminish the ER cross segments. In 16O + 194Pt response, we didn't watch any decrease in ER cross segment, which further affirmed that in this procedure the framework was advanced through the development of a genuine CN.

The present ER estimation gives additional proof to the impact of atomic dissemination in mass ~ 200 locale. Be that as it may, more exploratory outcomes are required to have a superior comprehension of the response elements in this mass area.

REFERENCES

[1] G. K. Mehta and A. P. Patro (1988). Nucl. Instr. what's more, Meth A 268, p. 334.

[2] D. Kanjilal, S. Chopra, M. M. Narayanan, I. S. Iyer, V. Jha, R. Joshi, and S. K. Datta (1993). Nucl. Instr. what's more, Meth A 328, p. 97.

[3] J. O. Stoner (2004). Nucl. Instr. what's more, Meth. A 521, p. 43.

[4] G. F. Meadow (1978). Radiation Detection and Measurements (John Wiley and Sons Inc, 1978).

[5] http:www.iuac.ernet.in/investigate/nuclear_physics/GPSC/GPSC_main.html (1990).

[6] A. Breskin, R. Chechik, Z. Fraenkel, P. Jacobs, I. Tserruya, and N. Zwang (1984). Nucl. Instr. what's more, Meth. A 221, p. 363.

[7] A. Jhingan, P. Sugathan, K. S. Golda, R. P. Singh, T. Varughese, H. Singh, B. R. Behera, and S. K. Mandal (2010). Rev. Sci. Instrum. 80, p. 123502.

[8] T. K. Ghosh, S. Buddy, T. Sinha, S. Chattopadhyay, K. S. Golda, and P. Bhattacharya (2005). Nucl. Instr. what's more, Meth. A 540, p. 285.

[9] B. P. AjithKumar, E. T. Subramaniam, K. Singh, and R. K. Bhowmik (1997). In Proceedings of SANAI-97, Trombay.

[10] A. K. Sinha, N. Madhavan, J. J. Das, P. Sugathan, D. O. Kataria, A. P. Patro, and G. K. Mehta (2010). Nucl. Instr. furthermore, Meth.A 339, p. 543.

[11] S. Nath and N. Madhavan (2006). In IUAC yearly report, area 4-3.3, pp. 103-105.

[12] N. Madhavan, S. Nath, P. Sugathan, J. J. Das, A. Jhingan, T. Varughese, R. Singh, K. M. Varier, M. C. Radhakrishna, and A. K. Sinha (2004). in Proceedings of DAE-BRNS Symposium on Nuclear Physics, Trombay, Vol. 47 A, p. 50.

[13] N. Madhavan, S. Nath, T. Varughese, J. Gehlot, A. Jhingan, P. Sugathan, A. K. Sinha, R. Singh, K. M. Varier, M. C. Radhakrishna, E. Prasad, S. Kalkal, G. Mohanto, J. J. Das, R. Kumar, R. P. Singh, S. Muralithar, R. K. Bhowmik, A. Roy, R. Kumar, S. K. Suman, A. Mandal, T. S. Datta, J. Chakko, A. Choudhury, U. G. Naik, A. J. Malayadri, M. Archunan, J. Zacharias, S. Rao, M. Kumar, P. Barua, E. T. Subramanian, K. Rani, B. P. A. Kumar, and K. S. Golda, Pramana (2010). Journel of Physics 75, No.2, p. 317.

[14] A. Jhingan, P. Sugathan, S. Barua, J. J. Das, T. Varughese, N. Madhavan, S. Nath, and P. V. Madhusudhana Rao (2004). Nucl. Instr. furthermore, Meth.A 526, p. 376.

[15] P. D. Shidling, N. M. Badiger, S. Nath, R. Kumar, A. Jhingan, R. P. Singh, P. Sugathan, S. Murlithar, N. Madhavan, A. K. Sinha, S. Buddy, S. Verma, K. Kalita, S.

Mandal, R. Singh, B. R. Behera, K. M. Varier, and M. C. Radhakrishna (2006). Phys. Rev. C 74, 064603.

Corresponding Author

Sonu Rani*

Research Scholar of OPJS University, Churu, Rajasthan